Available online at www.sciencedirect.com
ScienceDirect
Journal of Magnetic Resonance 186 (2007) 26–33
JMR Journal of Magnetic Resonance
www.elsevier.com/locate/jmr

The role of ^{15}N CSA and CSA/dipole cross-correlation in ^{15}N relaxation in solid proteins

Julien Sein [a], Nicolas Giraud [a], Martin Blackledge [b], Lyndon Emsley [a,*]

[a] Laboratoire de Chimie (UMR 5182 CNRS/ENS Lyon), Ecole Normale Supérieure de Lyon, 69364 Lyon, France
[b] Institut de Biologie Structurale Jean Pierre Ebel (UMR 5075 CNRS/CEA/UJF), 38027 Grenoble, France

Received 15 November 2006; revised 15 January 2007
Available online 20 January 2007

Abstract

The influence of the ^{15}N CSA on ^{15}N longitudinal relaxation is investigated for an amide group in solid proteins in powder form under MAS. This contribution is determined to be typically 20–33% of the overall longitudinal relaxation rate, at 11.74 and 16.45 T, respectively. The improved treatment is used to analyze the internal dynamics in the protein Crh, in the frame of a motional model of diffusion in a cone, using the explicit average sum approach. Significant variations with respect to the determined dynamics parameters are observed when properly accounting for the contribution of ^{15}N CSA fluctuations. In general, the fit of experimental data including CSA led to the determination of diffusion times (τ_w) which are longer than when considering only an ^{15}N–^{1}H dipolar relaxation mechanism. CSA-Dipole cross-correlation is shown to play little or no role in protonated solids, in direct contrast to the liquid state case.

Keywords: Nitrogen-15 longitudinal relaxation; Solid-state NMR; Protein dynamics; Cross-correlation; Magic angle spinning

1. Introduction

Recent breakthroughs in NMR assignment of microcrystalline protein samples [1,2] have opened the way toward detailed studies of backbone dynamics in proteins, and a few examples have already appeared, involving the first nitrogen-15 relaxation study of a microcrystalline, fully enriched protein [3], and subsequently the measurement of residual ^{2}H quadrupolar [4,5] or CH dipolar couplings [6], or ^{2}H relaxation [7]. These methods show a clear potential to establish a complete site-specific dynamic picture of proteins in crystals over a wide range of timescales. Notably, nuclear magnetic relaxation data recorded in solid proteins contain potentially very detailed information about local internal motions [3,8–13]. In particular, spin-lattice relaxation is mostly sensitive to motions occurring in the range of the ^{1}H and ^{15}N Larmor frequencies, that is on the picosecond to nanosecond timescale [13–15]. Several interactions can induce, through their fluctuations, a coupling between the spin system and the lattice. In the case of nitrogen-15 relaxation in a diamagnetic, uniformly labelled protein under magic angle spinning (MAS), we have recently shown using ^{1}H–^{15}N nuclear Overhauser effect measurements that the dominant relaxation mechanism is a stochastic modulation of the N–H dipolar interaction within the amide group [11]. It has also been shown that perturbations from additional protons, and from ^{15}N spin diffusion, can usually be neglected [16]. Using a theoretical description adapted for the orientation dependence of a powder undergoing MAS, and assuming the amide ^{1}H–^{15}N dipolar interaction as the only source of relaxation, parameters describing the internal dynamics were determined from experimental ^{15}N T_1 relaxation rates measured in two B_0 fields [12].

In this paper, we consider the additional contribution to ^{15}N relaxation due to chemical shift anisotropy (CSA) of the ^{15}N nucleus. We show that, as expected, and in analogy to what is observed in solution, the CSA contribution to the spin-lattice relaxation is not negligible, and

* Corresponding author. Fax: +33 4 72 72 88 60.
E-mail address: lyndon.emsley@ens-lyon.fr (L. Emsley).

1090-7807/$ - see front matter © 2007 Elsevier Inc. All rights reserved.
doi:10.1016/j.jmr.2007.01.010

we incorporate it into our analysis to improve the characterization of the internal dynamics in the protein Crh [17,18]. Finally, we discuss the possibility of a contribution from ^{15}N CSA—^{1}H–^{15}N dipole cross-correlation [19,20], and demonstrate that is should be absent in protonated proteins. The result is a fairly complete description of T_1 relaxation in the N–H group in solid proteins.

2. Longitudinal relaxation including CSA and dipolar relaxation mechanisms

We consider a nitrogen-15 nucleus in a peptide bond, and we assume that nitrogen-15 relaxation is induced both by the fluctuations of the dipolar interaction between the nitrogen-15 and its bound proton, and by the fluctuations of the coupling between the CSA of the nitrogen-15 atom and the external magnetic field B_0. We recall that the longitudinal relaxation rate, R_{1DD}, due to the dipolar ^{1}H–^{15}N interaction only, expressed in a static frame, reads [12,13]:

$$R_{1DD} = \frac{1}{4}\left(\frac{h}{2\pi}\frac{\gamma_H\gamma_N}{\langle r_{NH}\rangle^3}\right)^2 [J_0(\omega_H-\omega_N) + 3J_1(\omega_N) + 6J_2(\omega_H+\omega_N)] \quad (1)$$

where γ_H and γ_N are gyromagnetics ratios of ^{1}H and ^{15}N, respectively, and $\langle r_{NH}\rangle$ is the effective N–H distance (considering vibrational motions). For numerical calculations $\langle r_{NH}\rangle$ was set to 1.02 Å. $J_m(\omega)(m = 0, 1, 2)$ is a spectral density function, defined by:

$$J_m(\omega) = 2\int_0^\infty G_m(t)\cos(\omega t)\,dt \quad (2)$$

where $G_m(t)$ $(m = 0, \pm1, \pm2)$ is the autocorrelation function, which depends on the nature of the motion of the N–H interaction vector.

2.1. Expression of the CSA longitudinal relaxation rate

For the CSA contribution to the relaxation rate, we assume that the CSA tensor is axially symmetric, with principal values σ_x, σ_y and σ_z in its principal axis system. The z-axis of the tensor is assumed to be aligned with the direction of the internuclear N–H vector. The contribution of CSA to the longitudinal relaxation rate reads [21]:

$$R_{1CSA} = \frac{1}{3}\omega_N^2(\sigma_{//}-\sigma_\perp)^2 J_1(\omega_N) \quad (3)$$

where $\sigma_{//} = \sigma_z$ and $\sigma_\perp = \sigma_x = \sigma_y$. The frequency ω_N is the nitrogen-15 Larmor frequency. In numerical calculations, $(\sigma_{//} - \sigma_\perp)$ is set to -170 ppm, which is the average value usually proposed in the literature for the case of a ^{15}N nucleus in a peptide bond [22–25].

The expression of the longitudinal relaxation rate of nitrogen-15, accounting for the contribution of both ^{1}H–^{15}N dipolar and CSA fluctuations is then, with the same notations as above:

$$R_1 = \frac{1}{4}\left(\frac{\gamma_H\gamma_N}{\langle r_{NH}\rangle^3}\hbar\right)^2 [J_0(\omega_H-\omega_N) + 3J_1(\omega_N) + 6J_2(\omega_H+\omega_N)] + \frac{1}{3}\omega_N^2(\sigma_{//}-\sigma_\perp)^2 J_1(\omega_N) \quad (4)$$

Note that, despite the fact that this approximation is very widespread in this application, there is no particular evidence to support the assumption of a completely axially symmetric tensor for the nitrogen-15 chemical shift. Goldman showed that R_{1CSA} can be expressed for an asymmetric CSA tensor using the fact that such a tensor can be described through a sum of two axially symmetric tensors. Thus in the general case the CSA contribution can simply be written [26]:

$$R_{1CSA} = \frac{1}{3}\omega_N^2(\sigma_X^2+\sigma_Y^2+\sigma_Z^2-\sigma_X\sigma_Y-\sigma_Y\sigma_Z-\sigma_Z\sigma_X)J_1(\omega_N) \quad (5)$$

2.2. Calculation of the spectral density functions

In the following, we assume a motional model of the N–H internuclear vector wobbling in a cone. However, we point out that the following description could be used in exactly the same way for other motional models that might be used to describe the internal motion with greater accuracy. For the diffusion in a cone model, Lipari and Szabo proposed an approximation for the auto-correlation functions $G_m(t)$, which depend on the order m of the spherical harmonics [27]. In the solid-state, we recall that the absence of overall tumbling implies that we must evaluate individually $J_0(\omega)$, $J_{\pm1}(\omega)$ and $J_{\pm2}(\omega)$, in order to characterize the anisotropy of relaxation processes with respect to the external magnetic field [8,12,28]. The time-dependent orientation of the interaction vector in a powder under MAS is described through a series of reference frames: using the notations which have already been used elsewhere [12,28], we express the relevant autocorrelation functions in the laboratory frame, so as to link $G_m(t)$, (i.e., the description of the microscopic internal motion), to a "macroscopic" $C_a(t)$ function which determines the time scale of the relaxation phenomenon:

$$C_a(t) = \sum_{bb'=-2}^{2}\sum_{m=-2}^{2} D_{mb}^{(2)*}(\Omega_{CM})D_{mb'}^{(2)}(\Omega_{CM})D_{ba}^{(2)*} \times (\Omega_{ML})D_{b'a}^{(2)}(\Omega_{ML}) \times G_m(t) \quad (6)$$

with $a = 0, \pm1, \pm2$ and where $D_{ab}^{(2)}$ are Wigner rotation matrix elements and $D_{ab}^{(2)*}$ are the corresponding conjugate matrix elements. Ω_{CM} and Ω_{ML} are the Euler angles bringing the crystal frame C into coincidence with the magic angle frame M and the frame M into coincidence with the laboratory frame L, respectively. Eq. (6) implies two kinds of angular dependences for $C_a(t)$: on the one hand, for each crystallite, the relaxation rate is modulated by the variations of Ω_{ML} from 0 to 2π due to sample rotation at the

Magic Angle; on the other hand, the crystallite orientation in the rotor is described through the variations of Ω_{CM} [12]. R_1 in Eqs. (4) or (5) is therefore dependent on the crystallite orientation.

2.3. Contribution of the CSA fluctuations to R_1^{cryst}

Fig. 1 shows the calculated orientation dependence (without MAS) of the longitudinal relaxation rates $R_{1\ DD}^{cryst}$ (the longitudinal relaxation rate due only to the fluctuations of the ^1H–^{15}N dipolar interaction), and $R_{1DD+CSA}^{cryst}$ (longitudinal relaxation rate due to both dipolar and CSA interactions) for a N–H vector which diffuses in a cone, with a diffusion time $\tau_w = 1/6D_w = 6.6 \times 10^{-8}$ s and a semi-angle of (a) $\theta_0 = 11.2°$ and (b) $\theta_0 = 45°$, for a proton frequency of 700 MHz. We observe that $R_{1\ DD+CSA}^{cryst}$ has essentially the same orientation dependence as $R_{1\ DD}^{cryst}$. Indeed, $R_{1\ DD}^{cryst}$ and $R_{1\ DD+CSA}^{cryst}$ are both mainly influenced by the anisotropy of $J_1(\omega_N)$ which has a larger contribution than $J_0(\omega_H - \omega_N)$ and $J_2(\omega_H + \omega_N)$.

Fig. 2 shows the B_0 field dependence of the ratio $R_{1\ CSA}^{cryst}/R_{1\ DD+CSA}^{cryst}$ for an amide group in a single crystallite in the rotor, expressed in each plot as a function of rotor position and the orientation of the interaction vector with respect to the rotor axis. $R_{1\ CSA}^{cryst}$ is the longitudinal relaxation rate calculated from the contribution of the CSA alone. As expected, we notice that the higher the magnetic field, the bigger the contribution of the CSA: in particular, the ratio $R_{1\ CSA}^{cryst}/R_{1\ DD+CSA}^{cryst}$ reveals a maximum contribution of 33% at 16.45 T whereas for 11.8 T the maximum contribution of the CSA is 20%. Additionally, this figure illustrates the importance of $J_1(\omega_N)$ compared to $J_0(\omega_H - \omega_N)$ and $J_2(\omega_H + \omega_N)$, since only a small orientation dependence of the ratio $R_{1\ CSA}^{cryst}/R_{1\ DD+CSA}^{cryst}$ is observed (if J_0 and J_2 made no contribution, this graph would be flat).

2.4. CSA contribution to the generalized multi-exponential recovery curves

In a MAS experiment, each crystallite from a given carousel (defined by its orientation with respect to the rotor axis β_{CM}) undergoes an average relaxation rate R_1^{MAS} [8,12]:

$$R_1^{MAS}(\beta_{CM}) = \frac{1}{2\pi}\int_{\gamma_{CM}=0}^{2\pi} R_1^{cryst}(\gamma_{CM}, \beta_{CM})\, d\gamma_{CM}$$

Furthermore, the observed signal is the sum of the contributions of all the orientations of the crystallites with respect to the axis of the rotor. (This is referred to as the "Explicit Average Sum" (EAS) approach [12]). The intensity obtained is:

$$I^{exp}(t) = I_0^{exp}\frac{\int_{\beta_{CM}=0}^{\pi} \exp[-R_1^{MAS}(\beta_{CM})t]\sin(\beta_{CM})\, d\beta_{CM}}{\int_{\beta_{CM}=0}^{\pi}\sin(\beta_{CM})\, d\beta_{CM}} \quad (7a)$$

$I^{exp}(t)$ is evaluated through the computation of the following discrete sum over N_β crystallite orientations.

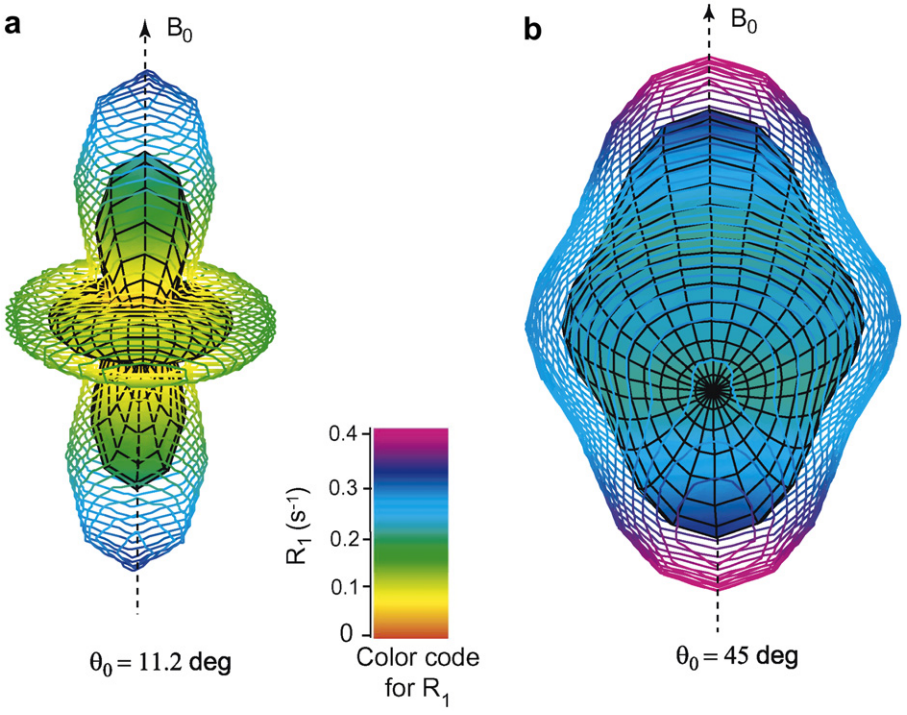

Fig. 1. Orientational dependence of the longitudinal relaxation rate for a nitrogen-15 nucleus bound to a proton, (without magic angle spinning), calculated with (contour style) and without (patch style) the contribution of CSA, for an external magnetic field of 16.45 T. The longitudinal relaxation rate is plotted for two motional amplitudes: (a) $\theta_0 = 11.2°$ and (b) $\theta_0 = 45.0°$, with $\tau_w = 6.6 \times 10^{-8}$ s, in spherical coordinates as a function of the orientation of the N–H vector with respect to the external magnetic field.

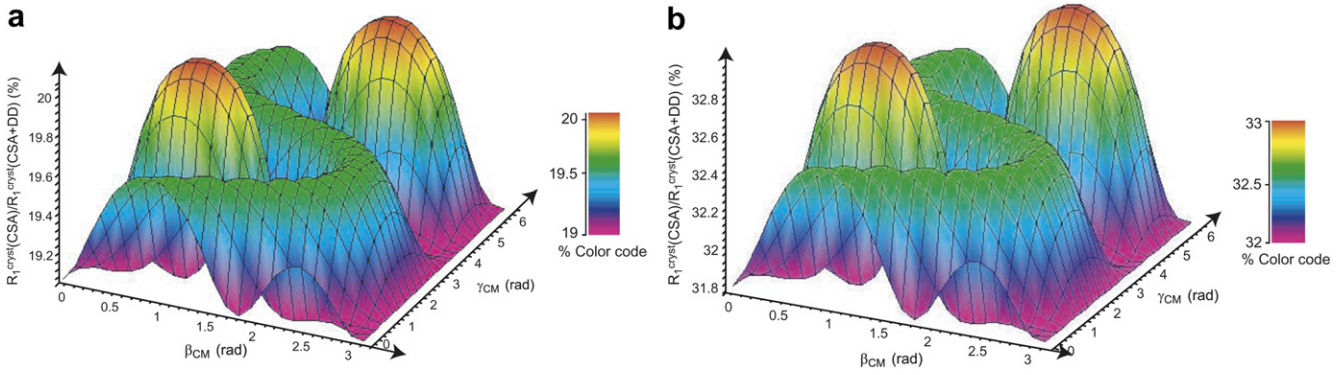

Fig. 2. $R_{1\ \mathrm{CSA}}^{\mathrm{cryst}}/R_{1\ \mathrm{DD+CSA}}^{\mathrm{cryst}}$ as a function of β_{CM} and γ_{CM} (orientations of the ^{15}N–^{1}H bond in the rotor frame) calculated for $\tau_w = 6.8\times10^{-8}$ s and $\theta_0 = 11.2°$(A) or $\tau_0 = 45°$(B) at proton frequencies of (a) 500 MHz and (b) 700 MHz.

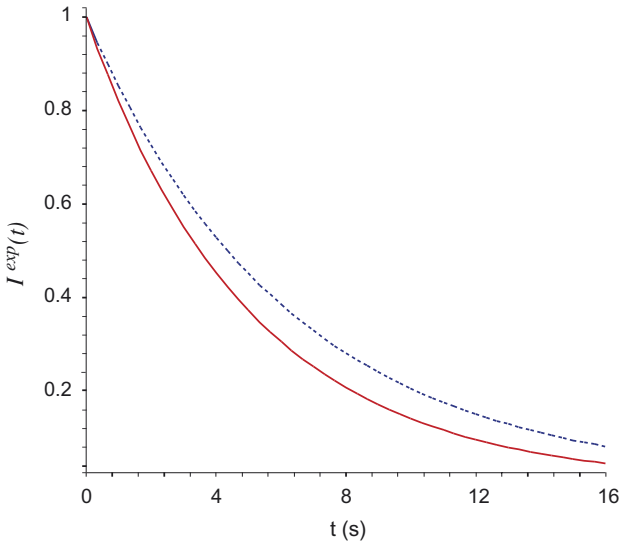

Fig. 3. Calculated relaxation curves for a NH group with (solid red curve) and without (dashed blue curve) the incorporation of CSA relaxation for $B_0 = 16.45$ T, with $\theta_0 = 45°$ and $\tau_w = 6.6\times10^{-8}$ s. The calculation was done by applying the EAS approach to Eq. (7b), with $N_\beta = 50$. (For interpretation of the references to color in this figure legend, the reader is referred to the web version of this paper.)

$$I^{\exp}(t) \approx I_0^{\exp} \times \frac{\sum_{b=0}^{N_\beta-1} \exp\left[-R_1^{\mathrm{MAS}}\left(\frac{(b+0.5)\pi}{N_\beta}\right)t\right] \sin\left(\frac{(b+0.5)\pi}{N_\beta}\right)}{\sum_{b=0}^{N_\beta-1} \sin\left(\frac{(b+0.5)\pi}{N_\beta}\right)} \tag{7b}$$

Fig. 3 shows the (multi-exponential) decaying curve of $I^{\exp}(t)$, calculated for a powder under MAS with and without the incorporation of the CSA contribution to the relaxation rate. As expected, we observe faster decay, i.e. a faster relaxation rate in the presence of CSA fluctuations.

3. Contribution of the CSA to the determination of dynamic parameters

To simplify the analysis of the behaviour of the decaying curves, we can extract a characteristic value of the longitudinal relaxation rate $R_1^{\mathrm{eff}}(\theta_0, \tau_w)$, which depends only on the dynamic parameters τ_w and θ_0, by fitting the multi-exponential curve $I^{\exp}(t)$ of a powder under MAS to a monoexponential function [12]. Fig. 4 shows a plot of $R_1^{\mathrm{eff}}(\theta_0, \tau_w)$ with the contribution of the dipolar and CSA interaction $R_{1\ \mathrm{CSA+DD}}^{\mathrm{eff}}(\theta_0, \tau_w)$, as a function of the N–H bond dynamics, at 500 and 700 MHz.

To quantify the contribution of the CSA fluctuations to the behavior of these curves, Fig. 5 shows a plot of the quantity $\frac{R_{1\ \mathrm{CSA+DD}}^{\mathrm{eff}} - R_{1\mathrm{DD}}^{\mathrm{eff}}}{R_{1\ \mathrm{CSA+DD}}^{\mathrm{eff}}}$, (a) at 500 MHz and (b) at 700 MHz.

The deviation in R_1^{eff} due to the CSA relaxation mechanism is slightly smaller for fast motion regimes (motions with τ_W typically smaller than 2×10^{-7} s), and reaches 19.5% and 32.5% at 500 and 700 MHz, respectively, for slower, less restricted motions.

3.1. Effect of CSA on experimentally determined dynamics

We have applied the EAS approach using both dipolar and CSA relaxation to determine dynamic probability distributions which account for both the experimental uncertainty, and the ability of the motional model to be constrained with the measurement of spin-lattice relaxation rates at two different fields [12]. The probability for a given N–H bond to diffuse in a cone of semi angle θ_0, with a diffusion time τ_w from the experimental measurement of the relaxation rate at two different fields (11.8 and 16.45 T), is proportional to:

$$P(\tau_w, \theta_0) \propto g(R_{1(11.7\ \mathrm{T})}^{\mathrm{eff}}(\tau_w, \theta_0), R_{1(11.74\ \mathrm{T})}^{\exp}) \times g(R_{1(16.45\ \mathrm{T})}^{\mathrm{eff}}(\tau_w, \theta_0), R_{1(16.45\ \mathrm{T})}^{\exp}) \tag{8}$$

where $R_1^{\exp}$ is the experimentally determined relaxation rate at a given magnetic field, $g(R_1, R_1^{\exp})$ is the distribution in the experimentally measured relaxation rates, and is assumed to be properly described by a gaussian distribution whose standard deviation is the experimental noise [12]. We account for the contribution of the ^{15}N CSA to ^{15}N relaxation by incorporating it into the computation of $R_1^{\mathrm{eff}}(\theta_0, \tau_w)$ as described in Eq. (4). The contour plots showing the calculated probabilities for 3 residues (Asp 38, Gly

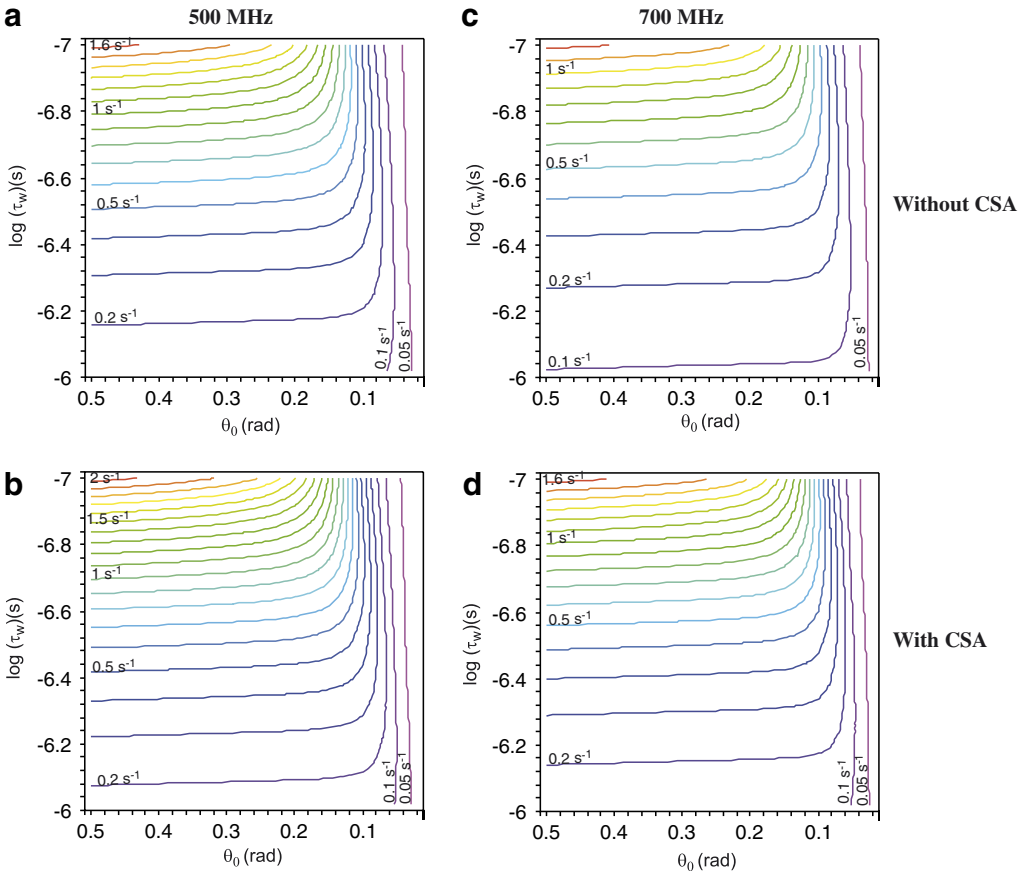

Fig. 4. Plot of the calculated longitudinal relaxation rate $R_1^{\text{eff}}(\theta_0, \tau_w)$ as a function of the dynamic parameters θ_0 and τ_w, (a) at 500 MHz without influence of CSA, (b) at 500 MHz with CSA, (c) at 700 MHz without influence of CSA, and (d) at 700 MHz with CSA. $R_1^{\text{eff}}(\theta_0, \tau_w)$ is calculated by fitting the simulated non-exponential relaxation curve for a powder under MAS with a monoexponential function, over a range of 15 s.

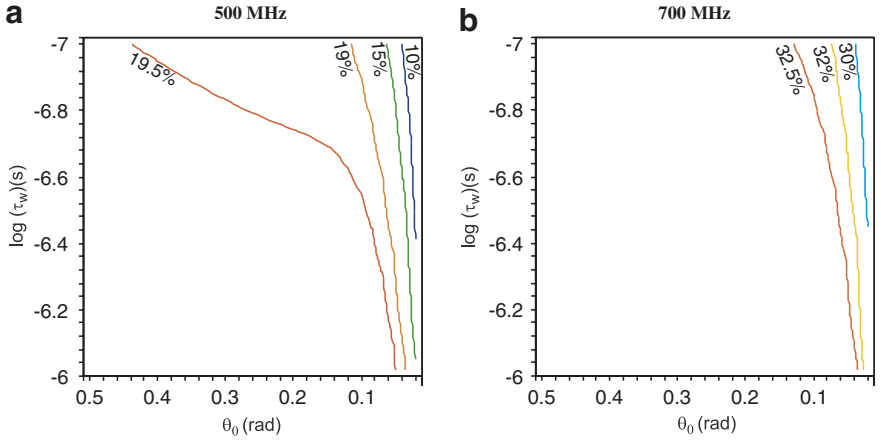

Fig. 5. Plot of the deviation $\frac{R_{1\ \text{CSA+DD}}^{\text{eff}} - R_{1\text{DD}}^{\text{eff}}}{R_{1\ \text{CSA+DD}}^{\text{eff}}}$ as a function of the N–H bond dynamics for proton frequencies of (a) 500 MHz and (b) 700 MHz.

39 and Lys 41) are displayed in Fig. 6. They were determined from the measurement of the ^{15}N T_1 at 500 and 700 MHz on microcrystalline Crh, as described elsewhere [12]. We note that the shape of the accuracy in the determination of the cone angle θ_0 is still poor from multi-field data for slower diffusion times.

Nevertheless, diffusion times are determined with a good accuracy from this data. Fig. 7 shows the comparison between the diffusion times determined, for a given amino acid, with and without the CSA contribution along the backbone. In general, the determined diffusion times are longer when the CSA contribution is accounted for. In

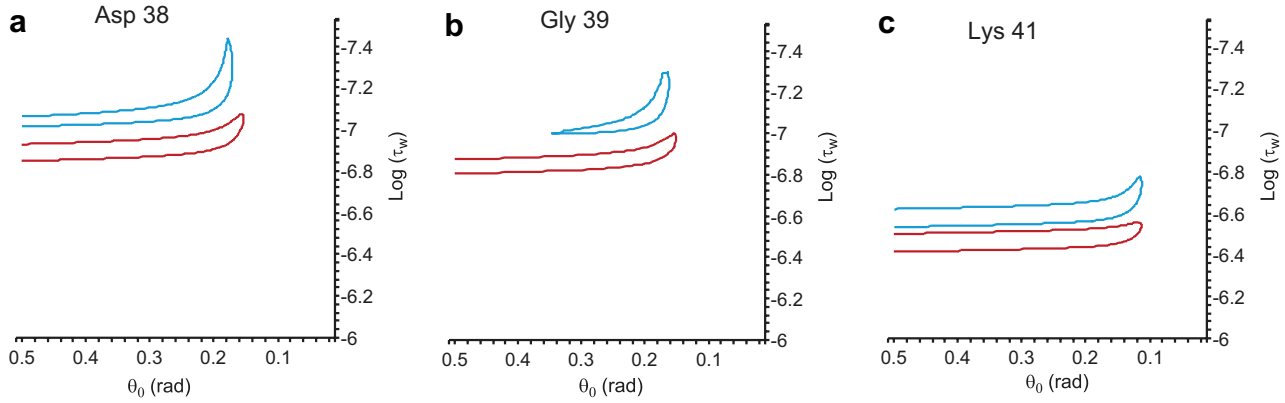

Fig. 6. Contour plot of the probability of dynamic parameters θ_0 and τ_w for 3 residues from experimentally determined relaxation rates. The probability distribution calculated from the model with and without CSA relaxation is displayed in red and blue, respectively. The contour is plotted for a probability of 90%. (For interpretation of the references to color in this figure legend, the reader is referred to the web version of this paper.)

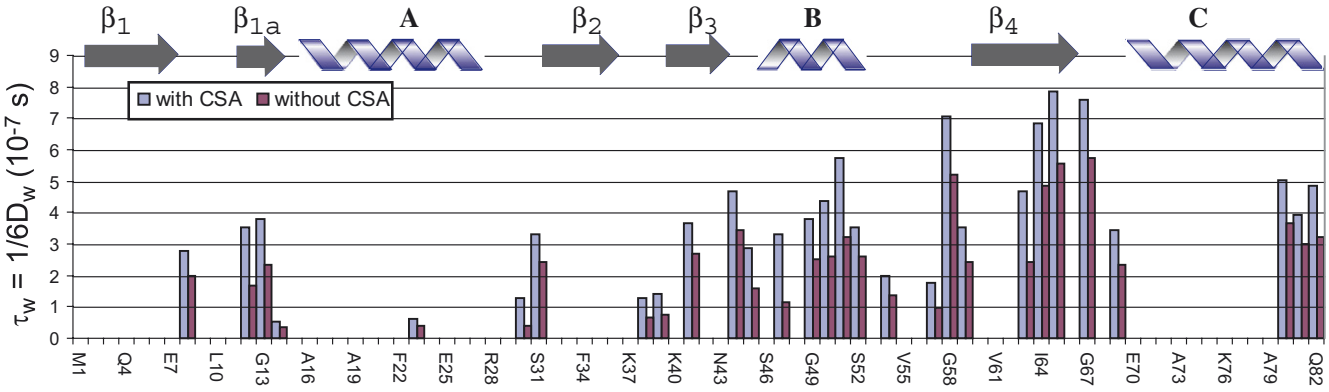

Fig. 7. Bar graph of the diffusion time τ_w determined for several residues in the protein Crh through the analysis of nitrogen-15 longitudinal relaxation rates at two different fields (11.74 and 16.45 T). The secondary structure of dimeric Crh is also shown (the uncertainty in the determination of the dynamic parameters, which reports on both the quality of the experimental data and the ability of the motional model to constrain spectral densities within a given dynamic regime, can be evaluated from the corresponding dynamic probability distributions, as discussed elsewhere [12]).

other words, neglecting CSA leads to determination of artificially faster dynamics.

4. Cross-correlation effects between ^{15}N CSA and the ^{15}N–^{1}H dipolar interaction

In the previous sections, we considered the case where the dipolar interaction and the ^{15}N CSA were treated independently. However, the symmetry and spatial dependence of these both interactions can be described by a set of second rank tensors, and their fluctuations both depend on the same internal motion of the N–H vector in the rotating frame [26]. Hence, interference can occur between H_D and H_{CSA}: this additional effect is referred to as cross-correlated relaxation and is at the root of many relaxation phenomena in macromolecules in solution [19,20,26]. In this study, we have shown that while the dipolar interaction is dominant, the contribution of the CSA of the ^{15}N nucleus is not much smaller and certainly should not be neglected: as a result, a significant contribution from cross-correlated relaxation could be expected. Furthermore, the strength of the cross-correlation, which depends on the relative intensity of the two interactions involved, is also a function of the orientation of the CSA tensor with respect to the N–H bond, and will be anisotropic.

The effect of cross-correlation will be to differentiate the relaxation of the two ^{15}N transitions in the N–H system with rates, $R_1^{(1)}$ and $R_1^{(2)}$, which correspond to ^{15}N interacting with the ^{1}H spin in its $|\alpha\rangle$ or $|\beta\rangle$ state [26]:

$$\begin{cases} R_1^{(1)} = R_{1\mathrm{DD+CSA}} + R_{1\mathrm{CC}} \\ R_1^{(2)} = R_{1\mathrm{DD+CSA}} - R_{1\mathrm{CC}} \end{cases} \tag{9}$$

where

$$R_{1\mathrm{CC}} = \frac{h\omega_{\mathrm{N}}(\sigma_{//} - \sigma_{\perp})\gamma_{\mathrm{N}}\gamma_{\mathrm{H}}}{2\pi r_{\mathrm{NH}}^3}\{J(\omega_{\mathrm{N}})\} \tag{10}$$

In this case, the decaying curve expected for a single crystallite is predicted to be biexponential:

$$N_Z(t) = \frac{1}{2}N_Z(0)\{\exp[-R_1^{(1)}t] + \exp[-R_1^{(2)}t]\} \tag{11}$$

This, if cross-correlation was active, and if we could measure the relaxation times of the two transitions of the N–H doublet independently, we would see different R_1 for each transition. Indeed we predict that the relaxation of each component of the ^{15}N doublet (doublet occurring

from the scalar coupling of ^{15}N and its bound proton) would occur (at 11.74 T, with $\tau_w = 6.6 \times 10^{-8}$ s and $\theta_0 = 11.2°$) with decay rates of 0.294 and 0.036 s^{-1}, while the monoexponential decay rate calculated by neglecting cross-correlation is 0.165 s^{-1}.

However, in the solid-state, the protons form a dense network of strongly dipolar coupled spins. This dipolar bath, which also mediates "spin diffusion", leads to a phenomenon known as "self decoupling" [29–32]. Notably, self decoupling interchanges the α and β states of the N–H doublet rapidly on the time scale of spin-lattice relaxation. Under static conditions, this effect can be large enough to actually partially decouple the doublet. This phenomenon is modified somewhat by magic angle spinning (if the system were weakly coupled, it would be removed by MAS), but, since the proton system is highly homogeneous [31,33]. Ernst et al. have shown that even under MAS the dominant residual term after averaging of the proton homonuclear Hamiltonian has the form [31]:

$$H_{II}^{(1)} = -\frac{i}{\omega_r} \sum_{i \neq j \neq k} \omega'_{ijk} I_{i,z} (I_j^+ I_k^- - I_j^- I_k^+) \tag{12}$$

This Hamiltonian will also induce exchange between the states of the NH doublet. Even for the rather weakly coupled case of adamantane, spin diffusion rates on the order of 300 s^{-1} were measured at 20 kHz MAS. As far as cross-correlation is concerned, this mechanism effectively plays the same role as applying π pulses during the relaxation delay, a method introduced by Kay et al. and Boyd et al. to suppress cross-correlation effects [34,35]. In consequence, due to proton spin diffusion, *the effects of cross-correlation should be absent in N–H relaxation in protonated proteins*. (Indeed, we so far see no evidence for cross-correlation effects, to within the signal to noise of the data for Crh).

Note that Eq. (10) decays only as the inverse of the spinning speed. Thus, it is unlikely that faster spinning will have a large effect on this conclusion [31]. Similarly, applying homonuclear dipolar decoupling techniques to reduce this effect does not appear currently practical over the length of the relaxation delay required here. In contrast, we would expect this effect to disappear in proteins containing *extremely high* levels of deuteration [36,37], sufficient to isolate the residual protons, and quench spin diffusion processes on the timescale of the relaxation times involved here (seconds). In this case, CSA/dipole cross-correlation effects would reappear in the spectrum. Note however that moderate deuteration is not sufficient to stop spin diffusion on this timescale.

5. Conclusion

The influence of the ^{15}N CSA on ^{15}N longitudinal relaxation in solid proteins under MAS was investigated. We have calculated the influence of ^{15}N CSA fluctuations on longitudinal relaxation in the simple case where an axially symmetric CSA tensor is aligned with the N–H bond vector. The more general case of an asymmetric CSA tensor was also addressed, and can be simply accounted for. The quantitative contribution of ^{15}N CSA to longitudinal relaxation was then estimated for an amide group in a protein, in powder form under MAS. This contribution was determined to be typically of 20% and 33% of the overall longitudinal relaxation rate, at 11.74 and 16.45 T, respectively. Furthermore, we have used this improved relaxation model to make an enhanced, quantitative analysis of the site specific internal dynamics in the protein Crh, for diffusion in a cone, using the EAS approach. We have observed significant variations of the determined dynamic parameters when properly accounting for the contribution of ^{15}N CSA fluctuations. In general, diffusion times τ_w were determined to be longer when including the effect of CSA.

Interestingly, CSA-Dipole cross-correlation is expected to play little or no role in protonated solids, in direct contrast to the liquid state case.

In conclusion, the analysis presented here, together with the ^1H–^{15}N nuclear Overhauser effects discussed previously [11], provides a more complete and accurate picture of longitudinal ^{15}N relaxation processes in solid proteins. This should notably allow detailed dynamics studies of solids proteins, using more interesting motional models, to be carried out in the future.

Acknowledgment

Financial support by the Access to Research Infrastructures activity in the 6th Framework Programme of the EC (Contract # RII3-026145, EU-NMR) for conducting the research is gratefully acknowledged.

References

[1] F. Castellani, van B. Rossum, A. Diehl, M. Schubert, K. Rehbein, H. Oschkinat, Structure of protein determined by solid-state magic-angle-spinning NMR spectroscopy, Nature 420 (2002) 98–102.
[2] A.E. McDermott, Structural and dynamic studies of proteins by solid-state NMR spectroscopy: rapid movement forward, Curr. Opin. Struct. Biol. 14 (5) (2004) 554–561.
[3] N. Giraud, A. Böckmann, A. Lesage, F. Penin, M. Blackledge, L. Emsley, Site-specific backbone dynamics from a crystalline protein by solid-state NMR spectroscopy, J. Am. Chem. Soc. 126 (37) (2004) 11422–11423.
[4] M. Hologne, Z.J. Chen, B. Reif, Characterization of dynamic processes using deuterium in uniformly H-2, C-13, N-15 enriched peptides by MAS solid-state NMR, J. Magn. Reson. 179 (1) (2006) 20–28.
[5] M. Hologne, K. Faelber, A. Diehl, B. Reif, Characterization of dynamics of perdeuterated proteins by MAS solid-state NMR, J. Am. Chem. Soc. 127 (32) (2005) 11208–11209.
[6] J.L. Lorieau, A.E. McDermott, Conformational flexibility of a microcrystalline globular protein: Order parameters by solid-state NMR spectroscopy, J. Am. Chem. Soc. 128 (35) (2006) 11505–11512.
[7] B. Reif, Y. Xue, V. Agarwal, M.S. Pavlova, M. Hologne, A. Diehl, Y.E. Ryabov, N.R. Skrynnikov, Protein side-chain dynamics observed by solution- and solid-state NMR: Comparative analysis of methyl H-2 relaxation data, J. Am. Chem. Soc. 128 (38) (2006) 12354–12355.
[8] A. Naito, S. Ganapathy, K. Akasaka, C.A. McDowell, Spin-lattice relaxation of C-13 in solid amino-acids using the Cp-Mas technique, J. Magn. Reson. 54 (2) (1983) 226–235.

[9] H.B.R. Cole, D. Torchia, An NMR study of the backbone dynamics of staphylococcal nuclease in the crystalline state, Chem. Phys. 158 (2–3) (1991) 271–281.
[10] A. Krushelnitsky, D. Reichert, Solid-state NMR and protein dynamics, Prog. Nucl. Magn. Reson. Spectrosc. 47 (1–2) (2005) 1–25.
[11] N. Giraud, J. Sein, G. Pintacuda, A. Böckmann, A. Lesage, M. Blackledge, L. Emsley, Observation of heteronuclear Overhauser effects confirms the 15N–1H dipolar relaxation mechanism in a crystalline protein, J. Am. Chem. Soc. 128 (38) (2006) 12398–12399.
[12] N. Giraud, M. Blackledge, M. Goldman, A. Böckmann, A. Lesage, F. Penin, L. Emsley, Quantitative analysis of backbone dynamics in a crystalline protein from nitrogen-15 spin-lattice relaxation, J. Am. Chem. Soc. 127 (51) (2005) 18190–18201.
[13] H.W. Spiess, Rotation of molecules and nuclear spin relaxation, in: P.F.E. Diehl, R. Kosfeld (Eds.), NMR Basic Principles and Progress, Springer Verlag, Berlin, Heidelberg, New York, 1978, p. 15.
[14] R.R. Ernst, G. Bodenhausen, A. Wokaun, Principles of Nuclear Magnetic Resonance in One and Two Dimensions, Clarendon Press, Oxford, 1987.
[15] M. Goldman, Formal theory of spin-lattice relaxation, J. Magn. Reson. 149 (2) (2001) 160–187.
[16] N. Giraud, M. Blackledge, A. Böckmann, L. Emsley, The influence of nitrogen-15 proton-driven spin diffusion on the measurement of nitrogen-15 longitudinal relaxation times, J. Magn. Reson. 184 (2006) 51–61.
[17] M. Juy, F. Penin, A. Favier, A. Galinier, R. Montserret, R. Haser, J. Deutscher, A. Böckmann, Dimerization of Crh by reversible 3D domain swapping induces structural adjustments to its monomeric homologue HPr, J. Mol. Biol. 332 (2003) 767–776.
[18] A. Böckmann, A. Lange, A. Galinier, S. Luca, N. Giraud, M. Juy, H. Heise, R. Montserret, F. Penin, M. Baldus, Solid state NMR sequential resonance assignments and conformational analysis of the 2×10.4 kDa dimeric form of the *Bacillus subtilis* protein Crh, J. Biomol. NMR 27 (4) (2003) 323–339.
[19] A. Kumar, R.C.R. Grace, P.K. Madhu, Cross-correlations in NMR, Prog. Nucl. Magn. Reson. Spectrosc. 37 (3) (2000) 191–319.
[20] P. Luginbuhl, K. Wuthrich, Semi-classical nuclear spin relaxation theory revisited for use with biological macromolecules, Prog. Nucl. Magn. Reson. Spectrosc. 40 (3) (2002) 199–247.
[21] M. Goldman, in: Quantum Description of High-Resolution NMR in Liquids, First ed., Oxford University Press, New York, 1988, p. 259.
[22] G. Cornilescu, A. Bax, Measurement of proton, nitrogen, and carbonyl chemical shielding anisotropies in a protein dissolved in a dilute liquid crystalline phase, J. Am. Chem. Soc. 122 (41) (2000) 10143–10154.
[23] N. Tjandra, A. Szabo, A. Bax, Protein backbone dynamics and N-15 chemical shift anisotropy from quantitative measurement of relaxation interference effects, J. Am. Chem. Soc. 118 (29) (1996) 6986–6991.
[24] C.H. Wu, A. Ramamoorthy, L.M. Gierasch, S.J. Opella, Simultaneous characterization of the amide 1H chemical shift, 1H–15N Dipolar, and 15N chemical shift interaction tensors in a peptide bond by three-dimensional solid-state NMR spectroscopy, J. Am. Chem. Soc. 117 (1995) 6148–6149.
[25] A.L. Lee, A.J. Wand, Assessing potential bias in the determination of rotational correlation times of proteins by NMR relaxation, J. Biomol. NMR 13 (2) (1999) 101–112.
[26] M. Goldman, Interference effects in the relaxation of a pair of unlike spin-1/2 nuclei, J. Magn. Reson. 60 (3) (1984) 437–452.
[27] G. Lipari, A. Szabo, Pade approximants to correlation-functions for restricted rotational diffusion, J. Chem. Phys. 75 (6) (1981) 2971–2976.
[28] D. Torchia, A. Szabo, Spin-lattice relaxation in solids, J. Magn. Reson. 49 (1982) 107–121.
[29] M. Mehring, Principles of High Resolution NMR in Solids, Springer Verlag New York Inc, Berlin, 1983.
[30] D. Suter, R.R. Ernst, Spin diffusion in resolved solid-state NMR-spectra, Phys. Rev. B 32 (9) (1985) 5608–5627.
[31] M. Ernst, A. Verhoeven, B.H. Meier, High-speed magic-angle spinning C-13 MAS NMR spectra of adamantane: Self-decoupling of the heteronuclear scalar interaction and proton spin diffusion, J. Magn. Reson. 130 (2) (1998) 176–185.
[32] B.H. Meier, Polarization transfer and spin diffusion in solid-state, Advances in Magnetic and Optical Resonance 18 (1994) 1–116.
[33] M.M. Maricq, J.S. Waugh, NMR in rotating solids, J. Chem. Phys. 70 (7) (1979) 3300–3316.
[34] L.E. Kay, L.K. Nicholson, F. Delaglio, A. Bax, D.A. Torchia, Pulse sequences for removal of the effects of cross-correlation between dipolar and chemical-shift anisotropy relaxation mechanism on the measurement of heteronuclear T1 and T2 values in proteins, J. Magn. Reson. 97 (2) (1992) 359–375.
[35] J. Boyd, U. Hommel, I.D. Campbell, Influence of cross-correlation between dipolar and anisotropic chemical-shift relaxation mechanisms upon longitudinal relaxation rates of N-15 in macromolecules, Chem. Phys. Lett. 175 (5) (1990) 477–482.
[36] M. Hologne, V. Chevelkov, B. Reif, Deuterated peptides and proteins in MAS solid-state NMR, Prog. Nucl. Magn. Reson. Spectrosc. 48 (4) (2006) 211–232.
[37] V. Chevelkov, K. Rehbein, A. Diehl, B. Reif, Ultrahigh resolution in proton solid-state NMR spectroscopy at high levels of deuteration, Angew. Chem. 45 (23) (2006) 3878–3881.